Available online at www.sciencedirect.com

SciVerse ScienceDirect

Ceramics International 39 (2013) 4783–4789

CERAMICS INTERNATIONAL

www.elsevier.com/locate/ceramint

Solid-state combustion synthesis of spinel $LiMn_2O_4$ using glucose as a fuel

Xianyan Zhou[a,b], Mimi Chen[a,b], Mingwu Xiang[a,b], Hongli Bai[a,b], Junming Guo[a,b,*]

[a]*Key Laboratory of Chemistry in Ethnic Medicinal Resources, State Ethnic Affairs Commission & Ministry of Education Kunming, Yunnan 650500, PR China*

[b]*School of Chemistry and Biotechnology, Yunnan University of Nationalities, Kunming, Yunnan 650500, PR China*

Received 6 October 2012; received in revised form 8 November 2012; accepted 22 November 2012
Available online 5 December 2012

Abstract

Spinel $LiMn_2O_4$ cathode material was rapidly synthesized in 1 h by solid-state combustion synthesis using metal carbonates as metal ion sources and glucose as a fuel. The effect of different amounts of glucose on the structure and electrochemical performance of as-prepared $LiMn_2O_4$ was investigated by X-ray diffraction (XRD), scanning electron micrographs (SEM), galvanostatic charge–discharge test, cyclic voltammetry (CV) and electrochemical impedance spectroscopy (EIS). $LiMn_2O_4$ spinel was identified as the main crystalline phase with the presence of minor Mn_3O_4. The amount of glucose greatly affected the formation of Mn_3O_4. The optimal content of glucose was found to be 10 wt%. Under this condition, the Mn_3O_4 peaks almost disappeared, and high-purity spinel $LiMn_2O_4$ was obtained. Its initial discharge specific capacity of was 125.9 mAh/g, and discharge specific capacity retained at 105.2 mAh/g after 40 cycles. The detail influence of glucose on the electrochemical activity, reversibility and cycling performance of $LiMn_2O_4$ was discussed.

Keywords: Solid-state combustion synthesis; Spinel $LiMn_2O_4$; Glucose; Electrochemical properties

1. Introduction

Lithium-ion battery is considered as an alternative to conventional power source for space devices, portable electronic devices, and electric vehicles (EV) owing to its high working voltage, long cycle lifespan as well as high energy density [1,2]. Currently, the cathode materials focus on layered structure $LiCoO_2$, $LiNiO_2$, $LiMnO_2$ and spinel $LiMn_2O_4$. Among these cathode materials, the $LiCoO_2$ is high cost, environmental risk, and limited abundance of cobalt have been recognized to be disadvantageous. In comparison, the spinel $LiMn_2O_4$ has been intensively investigated as a promising cathode material of lithium secondary batteries due to its excellent safety, low cost, non-toxicity, environmental friendly, easy preparation and excellent voltage profile characteristics [3–5].

Generally, the electrochemical performance of cathode material is affected by its morphology, phase homogeneity, crystallite size, etc. These aspects clearly depend on methods adopted for the synthesis [6,7]. Hence, an unabated interest has been shown by both the academic and the commercial sectors towards the selection of mode of synthesis and improvement in synthetic strategies for preparing cathode materials for lithium batteries. Many approaches, such as sol–gel method [8,9], solid-state reaction [10,11], hydrothermal method [12,13], and combustion synthesis [14,15] have been developed to prepare particulate cathode materials. Among these synthetic techniques, the solid-state reaction and combustion approach have attracted much attention as they show superior performance in producing high quality particles. But the former needs high temperature, long heating period meanwhile the reaction rate of the latter one is too fast, resulting in the control of the combustion reaction process difficult. Current research on the fabrication of single-phase spinel $LiMn_2O_4$ has been focused on developing a controllable

*Corresponding author. Tel./fax: +86 8715910014.
E-mail address: guojunming@tsinghua.org.cn (J. Guo).

0272-8842/$ - see front matter © 2012 Elsevier Ltd and Techna Group S.r.l. All rights reserved.
http://dx.doi.org/10.1016/j.ceramint.2012.11.068

method, characterizing the resultant particulate and improving its electrochemical properties. To date, the solid-state reaction and combustion synthesis of particulate spinel $LiMn_2O_4$ has been widely reported respectively. However, to the best of our knowledge, the direct synthesis of spinel $LiMn_2O_4$ has rarely reported by a solid-state combustion synthesis [16]. It integrates simplicity and easy mass production for solid-state synthesis and rapidity, low-cost for combustion synthesis, which is time and energy saving, and thus is promising for commercial application.

In this work, we extended our previous work to synthesize large-scale quantities of spinel $LiMn_2O_4$ products *via* a designed solid-state combustion method using glucose as a fuel. A desirable particulate size distribution of the spinel $LiMn_2O_4$ products can be obtained in 1 h by simply adjusting the amounts of glucose. The resultant spinel $LiMn_2O_4$ powders were characterized in detail and the effect of amount of glucose on physical and electrochemical properties of the $LiMn_2O_4$ cathode material was investigated.

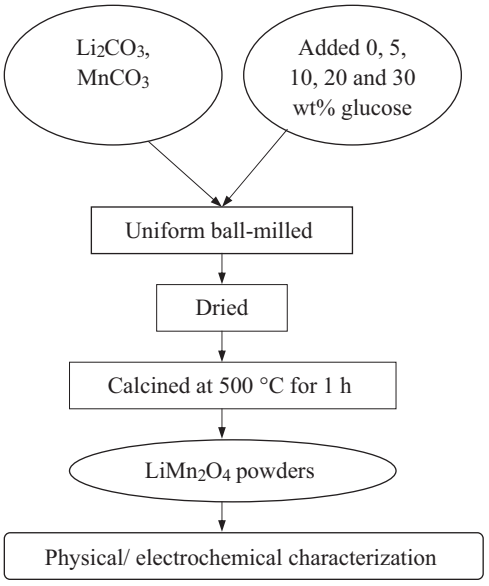

Fig. 1. The experimental procedure for synthesis of the $LiMn_2O_4$ products by solid-state combustion synthesis.

2. Experimental procedures

The source materials include lithium carbonate (AR), manganese carbonate (AR) and glucose (AR), which were purchased from Sinopharm Chemical Reagent Co., Ltd., Tianjin Kemiou Chemical Reagent Co., Ltd. and Tianjin No. 3 Chemical Reagent Factory, respectively. In a typical synthesis, lithium carbonate, manganese carbonate were firstly weighted and put into an agate jar with an ethanol medium at a predetermined molar ratio of Li:Mn = 1:2, in which lithium carbonate, manganese carbonate played as the lithium and manganese precursors. A given amount (0 wt%, 5 wt%, 10 wt%, 20 wt% and 30 wt % of gross weight) of glucose was added into the above mixture and then ball-milled it thoroughly. The alumina crucible with mixed starting materials was placed in a muffle furnace at 500 °C for 1 h. After the alumina crucible taken out of the muffle furnace and cooled down naturally to ambient temperature, the ultimate $LiMn_2O_4$ product was formed. The experimental procedure was depicted in Fig. 1.

The phase identification and structure of products were performed by the X-ray diffraction (D/max-TTRIII, Japan,). The diffraction data were collected at 40 kV and 200 mA with 2θ in the 10°–70° range. The Fourier transform infrared spectrometer (FT-IR) spectra of the as-prepared material was recorded as a KBr pellet in the region from 400 to 800 cm^{-1} with a Nicolet IS10 spectrometer. The morphologies of the as-prepared products were studied by scanning electron microscopy (QUANTA 200, America FEI).

Electrochemical measurements of the $LiMn_2O_4$ products were performed by assembling CR2025-type coin cell, which were assembled in a glove box filled with high-purity argon. The cells consist of a cathode and a lithium metal anode separated by a micro-porous polypropylene separator. The cathode was made by mixing the as-prepared $LiMn_2O_4$ with acetylene black and PVDF with a weight ratio of 8:1:1 in N-methyl-pyrrolidone (NMP) solution to form a syrupy mixture, then was coated on the pretreated aluminum foil. The film was dried at 80 °C for 4 h in an oven and then was vacuum dried at 120 °C for overnight before assembling to a cell. The electrolyte was 1 M $LiPF_6$ in EC/DMC (1:1 in volume) and Celgard 2320 film was used as separator. Galvanostatic charge–discharge experiments were performed using Land electric test system CT2001A (Wuhan Jinnuo Electronic Co., Ltd.) in the range of 3.2–4.35 V (versus Li/Li^+) at 0.2 C. Cyclic voltammogram (CV) was measured on an electrochemical workstation (IM6&Zennium, Zahner, Germany) at a scan rate of 0.2 mV/s between 3.2 and 4.35 V (versus Li/Li^+). Electrochemical impedance spectroscopy (EIS) measurement was carried out by applying an AC voltage of 10 mV amplitude over the frequency range after desired cycles.

3. Results and discussion

3.1. Structural analysis of product

Fig. 2 showed XRD patterns of the as-prepared $LiMn_2O_4$ products with different amounts of glucose at 500 °C. It can be seen from Fig. 2a and b that the diffractions occurred at $2\theta = 18.6°$, 36.1°, 37.7°, 43.9°, 48.0°, 58.1°, 63.8° and 67.1° were indexed to the characteristic diffractions of spinel $LiMn_2O_4$ [powder diffraction file (PDF) 35-0782], corresponding to its (111), (311), (222), (400), (331), (551), (440) and (531) planes, indicating the spinel $LiMn_2O_4$ as the main phase. In addition, very faint diffraction peaks at 28.9°, 32.4° and 59.9°corresponding to the diffractions of Mn_3O_4 (PDF 80-0382) can be observed. When only 10 wt% glucose was used (see Fig. 2c), the Mn_3O_4 peaks almost disappeared, and well-crystallized $LiMn_2O_4$ peaks appeared with space

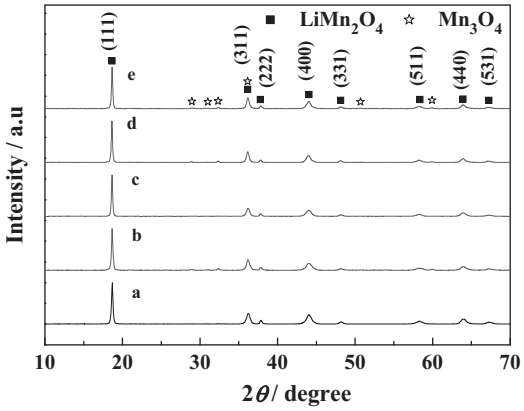

Fig. 2. X-ray diffraction patterns of the $LiMn_2O_4$ products with different amounts of glucose: (a) 0 wt%, (b) 5 wt%, (c) 10 wt%, (d) 20 wt% and (e) 30 wt%.

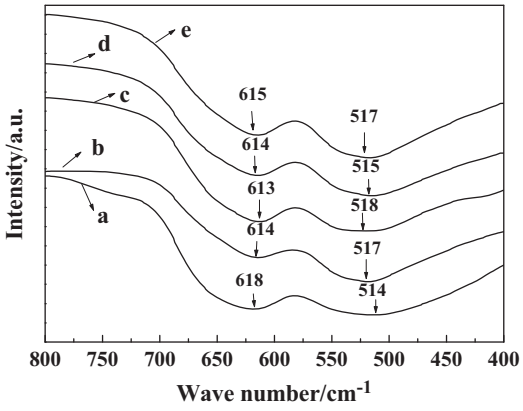

Fig. 3. FT-IR spectrum of the $LiMn_2O_4$ products prepared with different amounts of glucose: (a) 0 wt%, (b) 5 wt%, (c) 10 wt%, (d) 20 wt% and (e) 30 wt%.

group Fd3m. When the content of glucose increased to 30 wt% (Fig. 2e), the intensity of Mn_3O_4 diffraction peaks was the highest. The phenomena above indicated that the formation of impurity phase (Mn_3O_4) was affected by the content of glucose. During the synthesis process, the combustion of glucose was an exothermic reaction. When the $LiMn_2O_4$ preparation temperature set to be 500 °C, the true reaction temperature should be a little higher than the setting temperature due to the combustion of glucose [17]. When glucose was not added or added by 5 wt%, the formation of impurity phase (Mn_3O_4) indicated that the temperature is not high enough to realize full crystallization of $LiMn_2O_4$ [18]. When 10 wt% glucose used, the released heat from the combustion reaction elevated the reactant temperature to the optimum temperature for synthesis of $LiMn_2O_4$ and thus the relatively high-purity $LiMn_2O_4$ product was obtained [19]. When glucose was added by more than 20 wt%, the true reaction temperature might reach the decomposition temperature of $LiMn_2O_4$, resulting in the formation of the impurity Mn_3O_4 [20].

The calculated lattice parameters were 8.2061, 8.2122, 8.2138, 8.2187 and 8.2279 Å for $LiMn_2O_4$ with 0 wt%, 5 wt%, 10 wt%, 20 wt% and 30 wt% glucose used, respectively. The lattice parameter increased from 8.2061 to 8.2279 when the content of glucose increased from 0 wt% to 30 wt%. This small difference in lattice parameter was due to the higher glucose can release higher heat, so the true reaction temperature might became higher. The oxygen loss at higher reactant temperature accompanied with the side reaction $Mn^{4+} \rightarrow Mn^{3+}$, so a slight higher Mn^{3+} content and lower Mn^{4+} [21]. The radius for Mn^{3+} ions (0.72 Å) was larger than that of Mn^{4+} ion (0.67 Å). Therefore, a higher Mn^{3+}/Mn^{4+} ratio will result in a larger lattice parameter of $LiMn_2O_4$, as observed at higher content of glucose.

The FT-IR spectra of the products were displayed in Fig. 3. Two distinct absorption peaks at around 510 and 620 cm^{-1} were observed of different products. These bands are attributed to the Mn–O vibration mode due to the MnO_6 octahedrons, whereas the Li–O vibration mode, due to the LiO_4 tetrahedrons, lies within the region 200–400 cm^{-1}. These findings were quite similar to those given in earlier reports [22–24].

3.2. Morphological characterizations of products

The scanning electron microscopy (SEM) morphologies of $LiMn_2O_4$ products synthesized by solid-state combustion synthesis with different contents of glucose at 500 °C for 1 h were presented in Fig. 4. As shown in Fig. 4a, $LiMn_2O_4$ product prepared without glucose agglomerated seriously and the crystal size distribution was not uniform. The agglomeration of the sample decreased and the particle sizes increased with increasing contents of glucose. When 10 wt% glucose was used, the crystal size distribution was more uniform (see in Fig. 4c). But when glucose was added by more than 20 wt% (see in Fig. 4d and e), the agglomerations were very serious. The particle sizes of the $LiMn_2O_4$ products were more than 1 μm and the crystal size distribution was not uniform.

3.3. Electrochemical performance

Fig. 5 showed the typical charge–discharge capacity curves for the first cycle of the as-prepared $LiMn_2O_4$ products. The $LiMn_2O_4$ products were cycled at current density of 0.2 C rate in the potential range 3.2–4.35 V. It can be seen that the $LiMn_2O_4$ products prepared with and without the glucose had similar charge–discharge profiles, exhibiting two charge–discharge plateaus in the potential region of 3.9–4.20 V, which were ascribed to the remarkable characteristics of a well defined $LiMn_2O_4$ spinel and the voltage plateaus indicated that the insertion and extraction of lithium-ions occurred in two steps [25]. The first voltage plateau at about 3.95 V was attributed to the removal of lithium ions from half of the tetrahedral sites in which Li–Li interaction occurs. The second voltage plateau observed at around 4.15 V was ascribed to the removal of

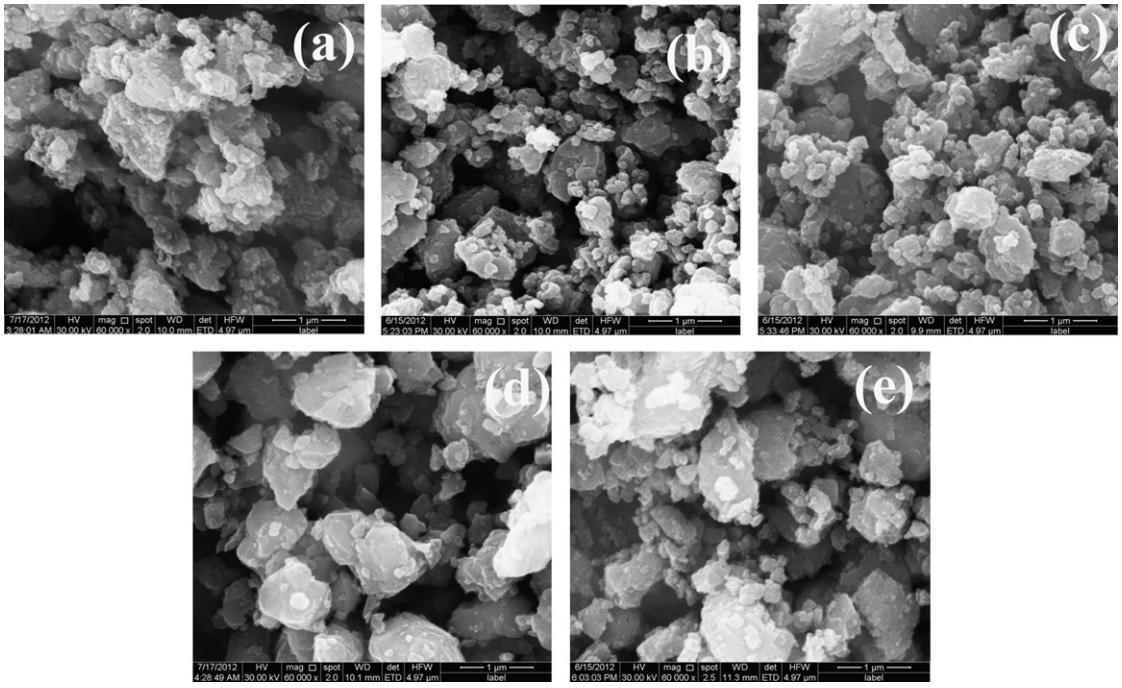

Fig. 4. SEM of the $LiMn_2O_4$ products with different amounts of glucose: (a) 0 wt%, (b) 5 wt%, (c) 10 wt%, (d) 20 wt% and (e) 30 wt%.

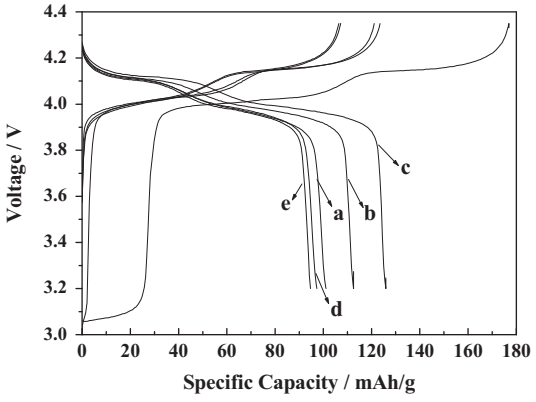

Fig. 5. The 1st charge–discharge curves of the $LiMn_2O_4$ products with different amounts of glucose: (a) 0 wt%, (b) 5 wt%, (c) 10 wt%, (d) 20 wt% and (e) 30 wt%.

lithium ions from the remaining tetrahedral sites. From Fig. 5 and Table 1, the initial discharge specific capacities of the $LiMn_2O_4$ products prepared with 0, 5, 10, 20 and 30 wt% glucose were 101.1, 112.5, 125.9, 97.3 and 94.7 mAh/g, respectively. It can be found that the optimum amount of glucose required for the preparation of $LiMn_2O_4$ powders with the maximum initial discharge capacity was 10 wt%. The results indicated appropriate content of glucose was contributed to a highest initial discharge specific capacity.

Fig. 6 displayed the variations of discharge capacity versus cycle number curves of the as-prepared $LiMn_2O_4$ products in the voltage range of 3.2–4.35 V at 0.2 C. As can be seen from the Fig. 6 and Table 1, the discharge specific capacities of the $LiMn_2O_4$ products prepared with 0, 5, 10, 20 and 30 wt% glucose after 40 cycles were 91.3, 97, 105.2, 86.6 and 86.4 mAh/g, respectively. The capacity retentions of the products after 40 cycles were about 90.3%, 86.2%, 83.6%, 89% and 91.2%, respectively. The capacity retention for the product with 30 wt% glucose was the highest, but their discharge specific capacity was the lowest. The discharge specific capacity of the $LiMn_2O_4$ product with 10 wt% glucose was 105.2 mAh/g after 40 cycles, which was higher than those of the other samples. Therefore, the $LiMn_2O_4$ product with 10 wt% glucose was optimal.

Fig. 7 showed cyclic voltammograms of the as-prepared $LiMn_2O_4$ products between 3.2 and 4.35 V at a scanning rate of 0.2 mV/s. It was clear that the $LiMn_2O_4$ products displayed two pairs of redox peaks in cyclic voltammogram, indicating that the electrochemical intercalation and de-intercalation reactions of lithium-ion proceed in two steps. The results were strongly consistent with two plateau potentials of the charge-discharge capacity curves in Fig. 5. Two pairs of redox peaks were in symmetry well-defined splitting, indicating that the intercalation and de-intercalation of lithium-ion in the spinel $LiMn_2O_4$ were reversible [26]. The sample with 10 wt% glucose additive annealed at 500 °C for 1 h had the highest current peaks, indicating the lowest internal resistance and better electrochemical reactivity.

Fig. 8 displayed the electrochemical impedance spectroscopy (EIS) of the as-synthesized $LiMn_2O_4$ products before cycling. The perturbation potential was 5 mV with frequencies from 0.01 Hz to 100 kHz. A semicircle in the high frequency region followed by a linear part in low frequency region can be observed. The semicircle in high frequency region was assigned to charge transfer resistance, which was the resistance of

Table 1
Discharge specific capacity and capacity retention of the $LiMn_2O_4$ products.

Products (different amounts of glucose)	Discharge specific capacity (mAh/g)		Capacity retention (%)
	First cycle	40th cycle	
$LiMn_2O_4$ (0 wt%)	101.1	91.3	90.3
$LiMn_2O_4$ (5 wt%)	112.5	97.0	86.2
$LiMn_2O_4$ (10 wt%)	125.9	105.2	83.6
$LiMn_2O_4$ (20 wt%)	97.3	86.6	89.0
$LiMn_2O_4$ (30 wt%)	94.7	86.4	91.2

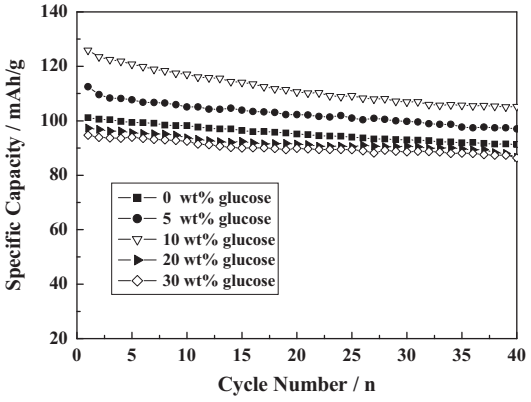

Fig. 6. Cycling performances of the $LiMn_2O_4$ products with different amounts of glucose: (a) 0 wt%, (b) 5 wt%, (c) 10 wt%, (d) 20 wt% and (e) 30 wt%.

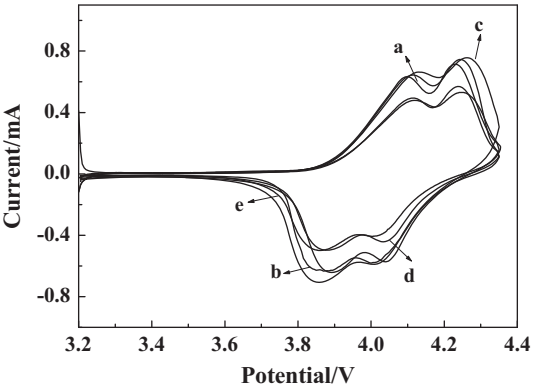

Fig. 7. Cyclic voltammograms of the $LiMn_2O_4$ products with different amounts of glucose: (a) 0 wt%, (b) 5 wt%, (c) 10 wt%, (d) 20 wt% and (e) 30 wt% between 3.2 and 4.35 V at scan rate of 0.2 mV/s.

charge transfer between surface film and spinel particles [27], and the straight line part corresponded to Warburg impedance, which was associated to lithium-ion diffusion in the $LiMn_2O_4$ particles [28]. The experimental impedance spectra were all fitted using the equivalent circuit shown in Fig. 9, where R_s was the electrolyte resistance, R_{ct} was the charge transfer resistance, C_{dl} denoted the double-layer capacitance, W was the Warburg impedance. Fitted results from EIS were displayed in Table 2. It can be seen from Table 2 that the variations of R_s was small for different amounts of glucose. The values of R_{ct} and W first decreased gradually to a

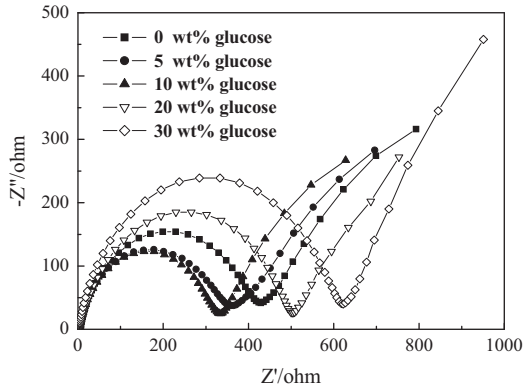

Fig. 8. EIS spectra of the $LiMn_2O_4$ products before charge–discharge.

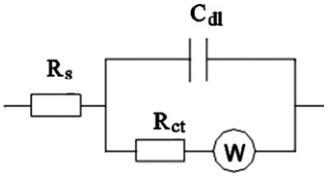

Fig. 9. Equivalent circuit of EIS.

minimum value when 10 wt% glucose was added and then increased with increasing glucose. The changed resistance was associated to electro-conduction and diffusion polarization. Smaller diffusion polarization and better electro-conduction resulting from better crystallinity and smaller particle size was the main reason why the sample with 10 wt% glucose had better activation performance and much higher initial discharge specific capacity as cathode material for lithium ion batteries.

4. Conclusions

Spinel $LiMn_2O_4$ was rapidly synthesized by solid-state combustion synthesis using metal carbonates as metal ion sources and glucose as a fuel. The effect of amount of glucose on the structure and electrochemical performance of $LiMn_2O_4$ powders was investigated. Spinel $LiMn_2O_4$ was identified as the main crystalline phase with presence of minor Mn_3O_4. The amount of glucose greatly affected the content of Mn_3O_4, which decreased at first and then increased with increasing

Table 2
The fitting values obtained from EIS.

Products (different amounts of glucose)	R_s (ohm)	R_{ct} (ohm)	W (ohm)
$LiMn_2O_4$ (0 wt%)	4.056	401.2	365.5
$LiMn_2O_4$ (5 wt%)	3.812	337.8	335.5
$LiMn_2O_4$ (10 wt%)	3.769	306.7	282.5
$LiMn_2O_4$ (20 wt%)	4.012	478.6	289.1
$LiMn_2O_4$ (30 wt%)	4.232	572.8	427.7

content of glucose. When the content of glucose reached 10 wt%, the Mn_3O_4 peaks almost disappeared, and well-crystallized $LiMn_2O_4$ peaks appeared with a space group Fd3m. Comprehensive considering the charge-discharge performance and EIS results, the optimal content of glucose is found to be 10 wt%. In this case, the initial discharge specific capacity was 125.9 mAh/g, and the discharge specific capacity retained at 105.2 mAh/g after 40 cycles. The better electrochemical performance was ascribed to the relative pure spinel $LiMn_2O_4$ crystalline phase and the uniform crystal size distribution.

Acknowledgments

This work was financially supported by the National Natural Science Foundation of China (51062018, 51262031), the Natural Science Foundation of Yunnan (2010FXW004), the Program for Innovative Research Team (in Science and Technology) in University of Yunnan Province (2010UY08, 2011UYN09).

References

[1] J.M. Tarascon, M. Armand, Issues and challenges facing rechargeable lithium batteries, Nature 414 (2001) 359–367.
[2] P.G. Balakrishnan, R. Ramesh, T.P. Kumar, Safety mechanisms in lithium-ion batteries, Journal of Power Sources 155 (2006) 401–414.
[3] D.W. Chung, N. Balke, S.V. Kalinin, R.E. Garcia, Virtual electrochemical strain microscopy of polycrystalline $LiCoO_2$ films, Journal of the Electrochemical Society 158 (2011) A1083–A1089.
[4] X.D. Li, W.S. Yang, D.G. Evans, X. Duan, Synthesis of layered $LiMnO_2$ by in situ oxidation intercalation and a study of the reaction mechanism and electrochemical performance, Chinese Science Bulletin 50 (2005) 213–216.
[5] J.M. Tarascon, E. Wang, F.K. Shokoohi, W.R. Mckinnon, S. Colson, The spinel phase of $LiMn_2O_4$ as a cathode in secondary lithium cells, Journal of the Electrochemical Society 138 (1991) 2859–2864.
[6] M.E. Spahr, P. Novak, B. Schnyder, O. Haas, R. Nesper, Characterization of layered lithium nickel manganese oxides synthesized by a novel oxidative co-precipitation method and their electrochemical performance as lithium insertion electrode materials, Journal of the Electrochemical Society 145 (1998) 1113–1121.
[7] L. Pascual, H. Gadjov, D. Kovacheva, K. Petrov, P. Herrero, J.M. Amarilla, R.M. Rojas, J.M. Rojo, Effect of the thermal treatment on the particle size and electrochemical response of $LiCr_{0.2}Mn_{1.8}O_4$ spinel, Journal of the Electrochemical Society 152 (2005) A301–A306.
[8] Y.L. Cui, W.J. Bao, Z. Yuan, Q.C. Zhuang, Z. Sun, Comparison of different soft chemical routes synthesis of submicro-$LiMn_2O_4$ and their influence on its electrochemical properties, Journal of Solid State Electrochemistry 16 (2012) 1551–1559.
[9] R. Dziembaj, M. Molenda, Stabilization of the spinel structure in $Li_{1+delta}Mn_{2-delta}O_4$ obtained by sol–gel method, Journal Of Power Sources 119 (2003) 121–124.
[10] W. Tang, L.L. Liu, S. Tian, L. Li, L.L. Li, Y.B. Yue, Y. Bai, Y.P. Wu, K. Zhu, R. Holze, $LiMn_2O_4$ nanorods as a super-fast cathode material for aqueous rechargeable lithium batteries, Electrochemistry Communications 13 (2011) 1159–1162.
[11] S.H. Ye, J.Y. Lv, X.P. Gao, F. Wu, D.Y. Song, Synthesis and electrochemical properties of $LiMn_2O_4$ spinel phase with nanostructure, Electrochimica Acta 49 (2004) 1623–1628.
[12] J. Huo, M. Wei, Characterization and magnetic properties of nanocrystalline nickel ferrite synthesized by hydrothermal method, Materials Letters 63 (2009) 1183–1184.
[13] X. Li, G. Wang, Low-temperature synthesis and growth of superparamagnetic $Zn_{0.5}Ni_{0.5}Fe_2O_4$ nanosized particles, Journal of Magnetism and Magnetic Materials 321 (2009) 1276–1279.
[14] K.M. Lee, H.J. Choi, J.G. Lee, Combustion synthesis of spinel $LiMn_2O_4$ cathode materials for lithium secondary batteries, Journal of Materials Science Letters 20 (2001) 1309–1311.
[15] Z.F. Dai, G.Y. Liu, B.S. Wang, D.W. Guo, Z.L. Huang, J.M. Guo, Solution combustion synthesis of $LiMn_2O_4$ powder by using glucose as fuel in acetate system, Journal of Functional Materials 39 (2008) 254–256.
[16] J.M. Guo, G.Y. Liu, X. Cui, Y. He, B.S. Wang, K.X. Chen, Effect of fuel content and temperature on spinel $LiMn_2O_4$ prepared by solid-state combustion synthesis, Rare Metal Materials and Engineering 38 (2009) 26–29.
[17] P.Z. Shen, D.Z. Jia, Y.D. Huang, L. Liu, Z.P. Guo, $LiMn_2O_4$ cathode materials synthesized by the cellulose-citric acid method for lithium ion batteries, Journal of Power Sources 158 (2006) 608–613.
[18] Y.P. Fu, Y.H. Su, C.H. Lin, S.H. Wu, Comparison of the microwave-induced combustion and solid-state reaction for the synthesis of $LiMn_2O_4$ powder and their electrochemical properties, Ceramics International 35 (2009) 3463–3468.
[19] Y.L. Ruan, Z.Y. Tang, E.S. Han, Synthesis and crystal structure of $LiMn_2O_4$ cathode material for Li-ion battery, Chinese Journal of Inorganic Chemistry 21 (2005) 232–236.
[20] Y.X. Wen, K.W. Zhou, H.F. Su, Z.F. Tong, Kinetics of the decomposition of $LiMn_2O_4$ in air, Journal of Inorganic Materials 20 (2005) 359–366.
[21] M. Yoshio, S. Inoue, M. Hyakutake, G. Piao, H. Nakamura, New lithium–manganese composite oxide for the cathode of rechargeable lithium batteries, Journal of Power Sources 34 (1991) 147–152.
[22] T.J. Richardson, S.J. Wen, K.A. Striebel, P.N. Ross, E.J. Cairns, FTIR spectroscopy of metal oxide insertion materials: analysis of $Li_xMn_2O_4$ spinel electrodes, Materials Research Bulletin 32 (1997) 609–618.
[23] C. Julien, M. Massot, Lattice vibrations of materials for lithium rechargeable batteries 1. Lithium manganese oxide spinel, Materials Science and Engineering B—Solid-State Materials for Advanced Technoloy 97 (2003) 217–230.
[24] S. Chitra, P. Kalyani, T. Mohan, Physical properties of $LiMn_2O_4$ spinel prepared at moderate temperature, Ionics 4 (1998) 8–15.

[25] K. Miura, A. Yamada, M. Tanaka, Electric states of spinel $Li_xMn_2O_4$ as a cathode of the rechargeable battery, Electrochimica Acta 41 (1996) 249–256.
[26] X.M. Wu, X.H. Li, M.F. Xu, Y.H. Zhang, Z.Q. He, Preparation of $LiMn_2O_4$ thin film by sol–gel method and its electrochemical properties, Chinese Journal of Power Sources 27 (2003) 376–378.
[27] R. Alcantara, M. Jaraba, P. Lavela, X-ray diffraction and electrochemical impedance spectroscopy study of zinc coated $LiNi_{0.5}Mn_{1.5}O_4$ electrodes, Journal of Electroanalytical Chemistry 566 (2004) 187–192.
[28] Y. Liu, X. Li, H. Guo, Z. Wang, Q. Hu, W. Peng, Y. Yang, Electrochemical performance and capacity fading reason of $LiMn_2O_4$/graphite batteries stored at room temperature, Journal of Power Sources 189 (2009) 721–725.